UNCONVENTIONAL VELOCITY SEISMIC PROCESSING BASED ON THE DIFFRACTION FILTER AND RESIDUAL DIFFRACTION MOVEOUT: APPLICATION TO A VIKING GRABEN DATASET

J. A. C. Gonzalez, J. J. S. de Figueiredo, T. A. Coimbra, J. Schleicher, and A. Novais

email: *jadsomjose@gmail.com*
keywords: *Diffraction Moveout, Diffraction Filtering, Remigration, PSDM, PSTM, Velocity Analysis*

ABSTRACT

Diffracted seismical waves are generated by unsmooth structures in the subsurface with size in the order of seismic wavelengths. Because the incident wavefield can be significantly affected by these discontinuities, many important properties of the corresponding seismic events can be used to improve the velocity-model building. In this paper, we develop a practical approach to construct velocity models in the time and depth domains using seismic diffractions. This methodology applies plane wave destruction (PWD) filters jointly with the residual diffraction moveout (RDM) method. Its only requirements are the presence of identifiable diffraction events after filtering out the reflection events and an arbitrary initial velocity model as input. We compare post-stack migrated images (in the time and depth domains) with images migrated with models obtained from conventional seismic processing. In both cases, we used post-stack Kirchhoff migration. Beyond the need to identify and select the diffraction events in the post-stack migrated sections in the depth domain, the method has a very low computational cost. The processing time to reach an acceptable velocity model was 75% less as compared with conventional processing. The applicability of our methodology was verified using a real Viking Graben seismic dataset.

INTRODUCTION

It is well known that when seismic waves interact with small structures in the subsurface of the earth (e.g., faults, fractures, channels, and rough edges of salt bodies), waves are scattered in all directions. The typical scattered signatures, known as diffractions, have been investigated for a long time with the purpose of understanding their signatures and how they could be used in seismic processing. Adequate usage of diffraction information in routine practice can be helpful in interpreting hydrocarbon traps in the subsurface and their final delineation (Tsingas et al., 2011). Special features exhibited by diffraction signatures (hyperbolae) have been particularly useful in the application of diffractions in velocity analysis (Sava et al., 2005; Novais et al., 2008; Landa and Reshef, 2009; Coimbra et al., 2013), super-resolution (Khaidukov et al., 2004), linear fracture imaging (Alonaizi et al., 2013) and CO_2 time-lapse monitoring (Alonaizi et al., 2014).

Reflections and diffractions are two types of coherent events generated in the subsurface. However, in conventional processing, most time is spent on reflections, while diffractions are considered noise due to their weak seismic energy. Particularly, conventional processing distorts the shape of a diffraction. Therefore, the true information about the structure contained in this kind of event (Zhang, 2004) is lost most of the time. Therefore, it is desirable to separate the reflected energy from the diffractions before carrying out the analysis of the latter.

Once the reflections have been filtered out, the diffracted energy is more accessible to further processing. In this work, we have implemented a diffraction filter based on plane-wave-destruction (PWD) filters (Claerbout, 1992; Fomel, 2009) with the local-slope correction developed by Schleicher et al. (2009). This correction is based on the fact that the slope's inverse can be extracted from the data in a fully analogous way to the slope itself. Combining the information of the slope and its inverse yields a simple but effective correction to the local slope. In our implementation of the PWD filters, we smooth over the so-extracted local slopes. Other slope-extraction methods are discussed in Hale (2007).

After filtering out the reflections, we then performed a velocity analysis on seismic diffraction panels. Our velocity analysis was based on the residual-diffraction-moveout (RDM) technique developed by Coimbra et al. (2013). The method was originally developed for zero-offset data. Here, we apply it to a stacked section and a near-offset section. The error resulting from the applying the method to a non-zero offset section is overcome after very few iterations. The number of necessary iterations depends on the complexity of the dataset. Finally, we compare the migrated seismic images (in the time and depth domains) obtained by conventional seismic processing with those obtained by the our processing sequence using RDM velocity analysis (which we will refer to as RDM processing). An application of RDM processing to a real Viking Graben seismic dataset confirms the applicability of our method.

METHODOLOGY

In this section, we describe our methodology for the analysis based on residual-diffraction-moveout (RDM) processing. The corresponding processing sequence makes use of plane-wave-destruction (PWD) filters to separate diffractions from reflections in near-offset sections before RDM velocity analysis. After the separation, the method uses the residual moveout of incorrectly migrated diffraction events in depth domain to update the velocity model. Although the theory is developed for zero-offset sections, we started the procedure with a near-offset section and used a normal-moveout (NMO) stacked section in the next iteration. The resulting error is negligible after very few iterations.

PWD filter and local slope

The RDM method uses the information carried by incorrectly migrated diffractions to determine updates for the velocity model. However, it is well known that reflection energy is dominant over diffraction energy. Therefore, it is necessary to separate or attenuate the reflections against the diffractions, if we want to use diffractions in seismic processing. According to Claerbout (1992), a plane-wave destruction (PWD) filter can be used to attenuate the nearly planar events associated with reflections. Such a PWD filter can be defined by means of the local plane-wave differential equation given by

$$\frac{\partial P}{\partial x} + \sigma \frac{\partial P}{\partial t} = 0, \tag{1}$$

where P is the wavefront that depends on offset x, time t, and the local-slope parameter σ. To implement a PWD filter according to equation (1), we need an estimate of σ. Then, by considering only a slowly varying background slope field, we can filter out the events with an almost constant slope, which are most likely reflections, and preserve events with stronger slope variations, which will include diffractions.

To determine the local slope σ at a point (x_i, t_j) in the data section, Claerbout (1992) suggested to use an iterative method to find the data residual, i.e., those parts of the data that do not satisfy equation (1). This residual is given by

$$R(\sigma) = \sum_{i,j}^{W} \left(\frac{\partial P(x_i, t_j)}{\partial x} + \sigma \frac{\partial P(x_i, t_j)}{\partial t} \right)^2, \tag{2}$$

where W is the size of windows selected around of the point (x_i, t_j). Fomel (2009) implemented an all-pass filter to find a similar solution using a finite-difference approximation of equation (1) in the frequency domain, although this process required high computational resources. For this reason, we used the simpler method of Schleicher et al. (2009) to estimate σ and the quadratic residual $R(\sigma)$.

The idea of the work of Schleicher et al. (2009) is to apply the original procedure of Claerbout (1992) twice. For the second application, they rewrite equation 1 as

$$q\frac{\partial P}{\partial x} + \frac{\partial P}{\partial t} = 0, \tag{3}$$

where $q = 1/\sigma$. Then, in correspondence to the technique of Claerbout (1992), the quadratic residual is given by

$$R(q) = \sum_{i,j}^{W} \left(q\frac{\partial P(x_i,t_j)}{\partial x} + \frac{\partial P(x_i,t_j)}{\partial t} \right)^2 . \tag{4}$$

The results of equations 2 and 4 can be combined to provide a simple and effective correction of the local-slope measure. According to Schleicher et al. (2009), the least-squares value of σ is given by

$$\langle \sigma \rangle_E = S \left(\sqrt{\frac{\sum_{i,j}^{W} \left(\frac{\partial P(x_i,t_j)}{\partial x} \right)^2}{\sum_{i,j}^{W} \left(\frac{\partial P(x_i,t_j)}{\partial t} \right)^2}} \right), \tag{5}$$

where S is defined as

$$S = -\mathrm{sgn} \left(\sum_{i,j}^{W} \left(\frac{\partial P(x_i,t_j)}{\partial x} \right) \left(\frac{\partial P(x_i,t_j)}{\partial t} \right) \right). \tag{6}$$

Equation (4) minimizes the error of the least-squares solution of both equations (2) and (4) simultaneously. To implement equation (1), any method can be used to estimate the slope, as long as a good estimate of this seismic parameter can be obtained.

Before applying our RDM processing sequence to real data, we performed several tests of PWD filters on synthetic data. Figure 1a shows the Sigsbee2B dataset used to test our PWD filter. Figure 1b is the local-slope panel estimated and Figure 1c is the diffraction panel after PWD filter application. We can see in Figure 1c that the energy of planar events is reduced and that the energy of diffraction events is more visible. Note that perfect removal of reflected energy is not required by the RDM method. It is only necessary that diffraction events can be identified and interpreted.

RDM analysis

Recently, Coimbra et al. (2013) developed a method for diffraction-point imaging and local migration velocity improvement based on the localization and picking of the residual moveout of incorrectly migrated diffraction events in the depth domain. Here, we apply this methodology to construct velocity models in both the depth and time domains.

According to Coimbra et al. (2013), considering a diffraction point at the true position (x_t, z_t) in a constant-velocity medium with true velocity v_t, the residual moveout of a diffraction event after of depth migration with an incorrect velocity v_0 coincides with the Huygens image-wave for the depth remigration from velocity v_t to v_0. The location of the Huygen's image-wave is defined as the curve or surface of all points where a possible event of the image point (x_t, z_t) might be placed when the migration velocity is changed from v_t to v_0 (Hubral et al., 1996). As a consequence, if the migration velocity is higher than the true medium velocity, an overmigrated diffraction event will have shape of an ellipse or if the migration velocity is smaller, the shape of an undermigrated diffraction event is a hyperbola. Mathematically, the resulting curve is given by (Hubral et al., 1996)

$$\frac{z^2}{v_0^2} + \frac{(x - x_t)^2}{v_0^2 - v_t^2} = \frac{z_t^2}{v_t^2}. \tag{7}$$

To emphasize the hyperbolic or elliptic shapes, Coimbra et al. (2013) rewrite equation 7 in the form

$$\frac{z^2}{b^2} + s\frac{(x - x_t)^2}{a^2} = 1, \tag{8}$$

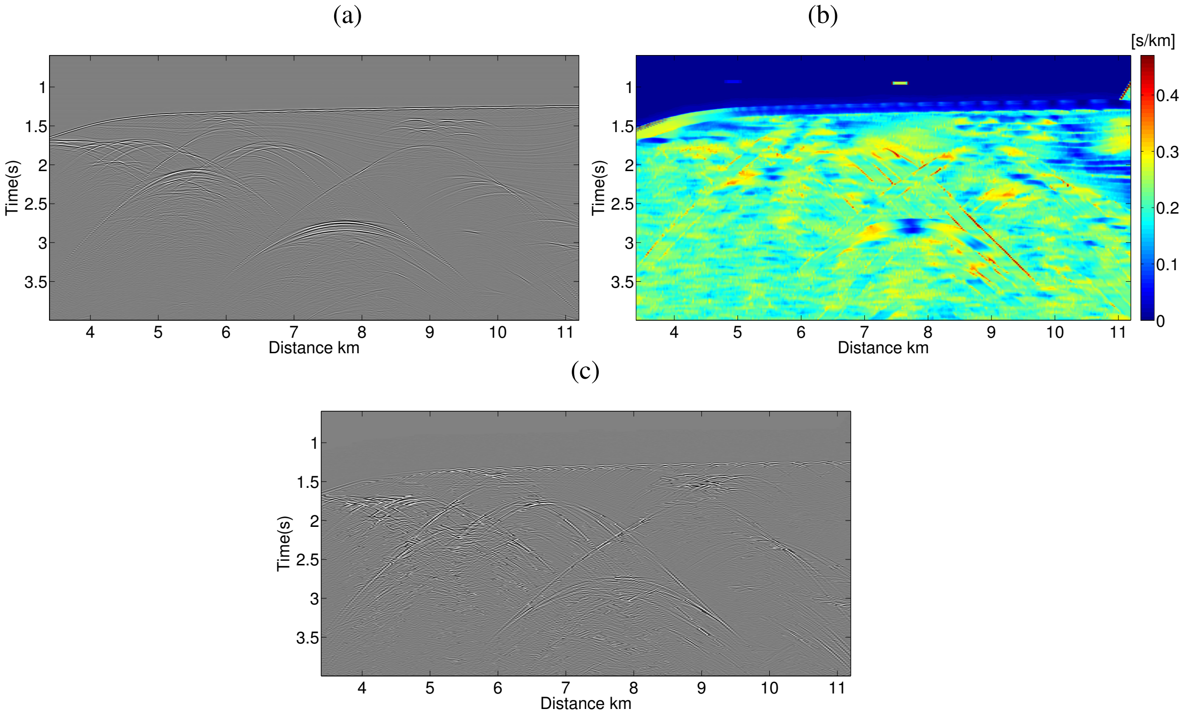

Figure 1: (a) The Sigsbee2B synthetic dataset. (b) Local-slopes panel. (c) Diffraction section PWD filter application.

where the half-axes a and b are given by

$$a = \frac{z_t}{v_t}\sqrt{|v_0^2 - v_t^2|} \quad \text{and} \quad b = \frac{z_t}{v_t} v_0. \tag{9}$$

Depending on the sign $s = sgn(v_0^2 - v_t^2) = sgn(v_o - v_t)$ equation 8 can represent an ellipse or a hyperbola.

Coimbra et al. (2013) used a least-squares method to find the best-fitting hyperbola or ellipse to describe an incorrectly migrated diffraction event. This provides estimates for the half-axes a and b as well as the horizontal coordinate of the apex x_t. Note that the a and b parameter are related to the slope of incorrectly migrated diffraction.

In a medium with a strong velocity gradient, this slope can be quite affected. To allow for stronger velocity gradients, Coimbra et al. (2013) modified equation (8) to

$$\frac{z^2}{b^2} + s\frac{(x - x_t)^2}{a^2} = 1 + \epsilon\,(x - x_t)\,z, \tag{10}$$

where $\epsilon(x - x_t)z$ is a perturbation term to allow for a rotation of the ellipse or hyperbola. The parameter ϵ is adjusted simultaneously with the other parameters of the ellipse or hyperbola in the least-squares procedure, but not used in the velocity-updating procedure.

The residual moveout of the incorrectly migrated diffraction events can then be used to update the migration velocity model. According to Coimbra et al. (2013) there are two ways to update the velocity model. One of them is related to the half-axes and the other one is using remigration trajectories, i.e., the curves connecting all positions where a migrated point can be found for different migration velocities. More details about the RDM method can be found in Coimbra et al. (2013).

Figure 2 shows a pictorial illustration of under- and overmigrated diffraction curves (black lines) with remigration trajectories (red lines). The black lines in Figure 2c and 2d are the hyperbola and the ellipse described by equations 8 and 9.

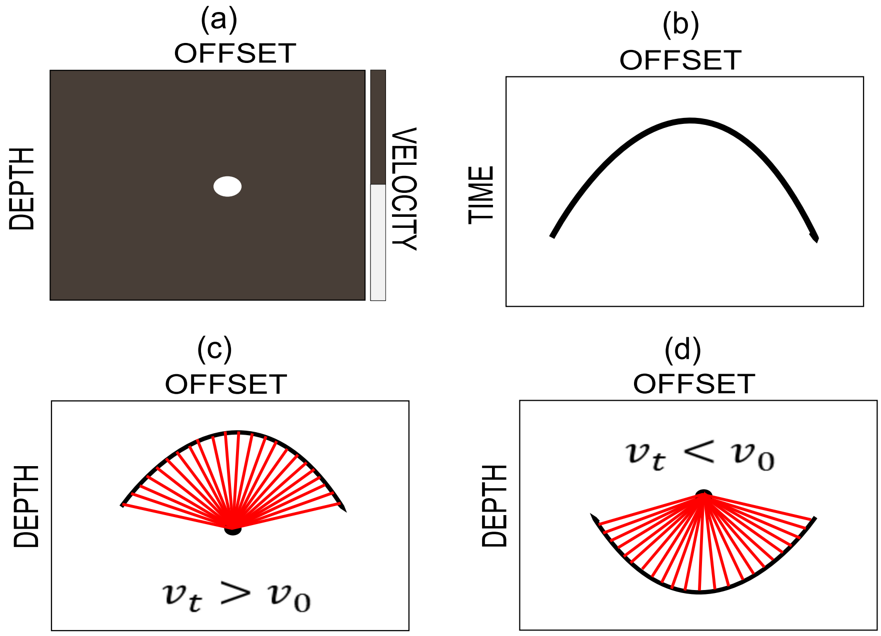

Figure 2: Pictorial illustration of incorrectly migrated diffraction events and remigration trajectories. (a) Constant velocity model with a scattering point located at the center of the model. (b) Zero-offset section over this diffraction point. (c) Remigration trajectories (red line) starting at an undermigrated hyperbolic diffraction curve (black line). (d) Remigration trajectories (red line) starting at an overmigrated elliptic diffraction curve (black line).

RDM processing

We combined the PWD filtering with the RDM velocity analysis into a new processing sequence for seismic diffractions. The new RDM processing to construct a velocity model, starting from a nearest-offset section, applies the PWD filter to separate diffraction events, and applies the residual diffraction moveout method to obtain a velocity model. The flowchart is depicted in Figure 3. Specifically, RDM processing consists of the following steps:

1. Pre-processing (geometry correction, trace editing, deconvolution, band-pass filtering and AGC) of the (real) dataset. This work was performed for the conventional and RDM processing.
2. Selection of the nearest-offset gather from the real dataset.
3. Calculation of the local slope for each point in the nearest-offset gather.
4. Application of the PWD filter to separate diffractions from reflections in the nearest-offset gather.
5. Migration of filtered diffractions using a constant velocity model with $v = 1500$ m/s.
6. Application of RDM velocity analysis using this migrated gather to find the first velocity model.
7. Application of an NMO stack with the current velocity model to the full dataset to obtain an improved ZO section, input to the next iteration.
8. Calculation of the local slope for each point in the current ZO section.
9. Application of the PWD filter to separate diffractions from reflections in the current ZO section.
10. Migration of filtered diffractions using the current velocity model.
11. Application of RDM velocity analysis on this gather to update the current velocity model.
12. Iteration of steps 7 to 11 until all identifiable diffractions are collapsed.
13. Depth and time migration of the final stacked section with the conventional and RDM velocity models.

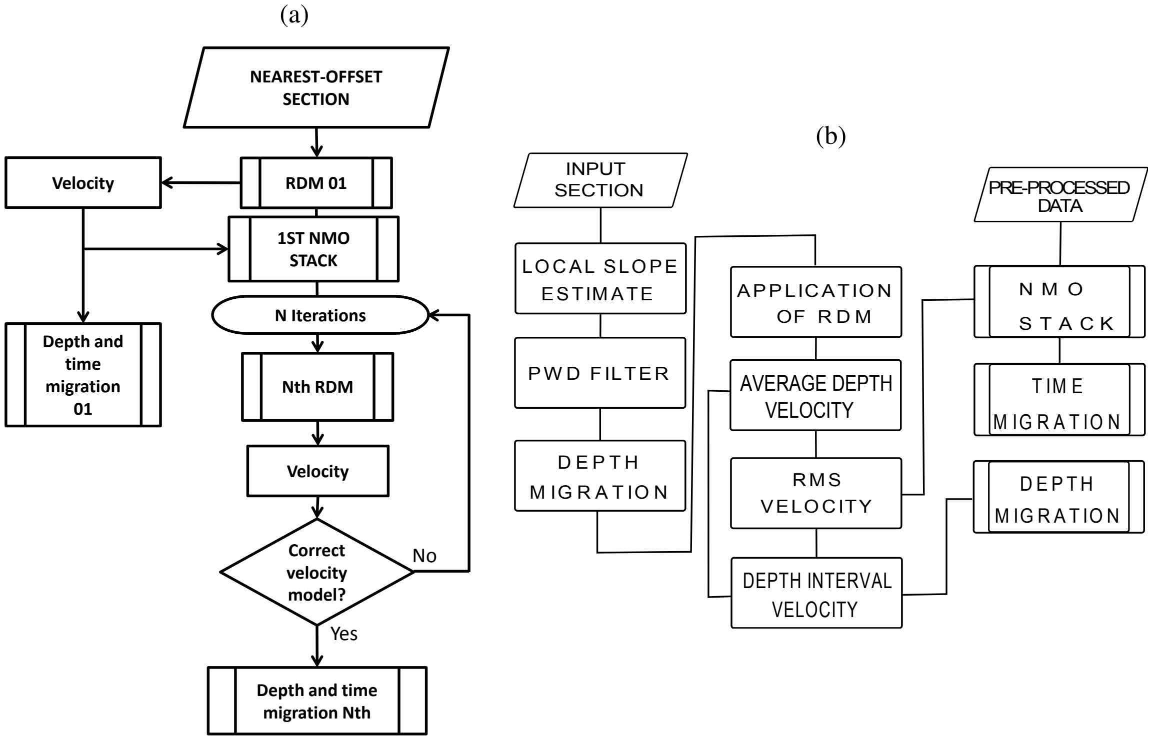

Figure 3: Processing flowcharts. (a) RDM processing sequence. (b) RDM velocity analysis.

In our application of the above processing sequence to a real Viking-Graben dataset, only two iterations of the above procedure (one with the nearest-offset gather, one with the first NMO-stacked section) were necessary to find an acceptable migration-velocity model. Other data may require more than two iterations. It is to be expected that the number of required iterations will depend on the complexity of the data.

THE VIKING-GRABEN DATASET

In this work, we have applied our new RDM-based processing sequence to a real dataset from the Viking Graben in the North Sea Basin, provided by Exxon Mobil.

Dataset description

The cited Viking Graben dataset was acquired with 1001 shot points and 120 channels. The sampling rate was 4 ms and the total recording time was 6 s. The distance between the shot points and between the receivers was 25 m. The minimum and maximum offsets were 262 m and 3237 m, respectively. The water depth along the seismic line was a relatively constant 300 m. The data contain a large number of diffraction events, which makes them is particularly well suited for an application of the RDM method. In geological terms, the presence of many diffraction events in the data means that there are many faults and discontinuities in the subsurface.

Preprocessing

The pre-processing steps consisted of trace muting, bandpass filtering with a zero-phase (6-12-50-70 Hz) Ormsby filter, and spherical divergence corrections. Moreover, these data need preprocessing to eliminate the water-bottom multiples before applying our methodology. We applied predictive deconvolution with 320 ms operator length and 20 ms prediction operator. Also, we used deconvolution with white noise (S/N=0.1) and predictive deconvolution to improve the amplitude resolution.

(a)

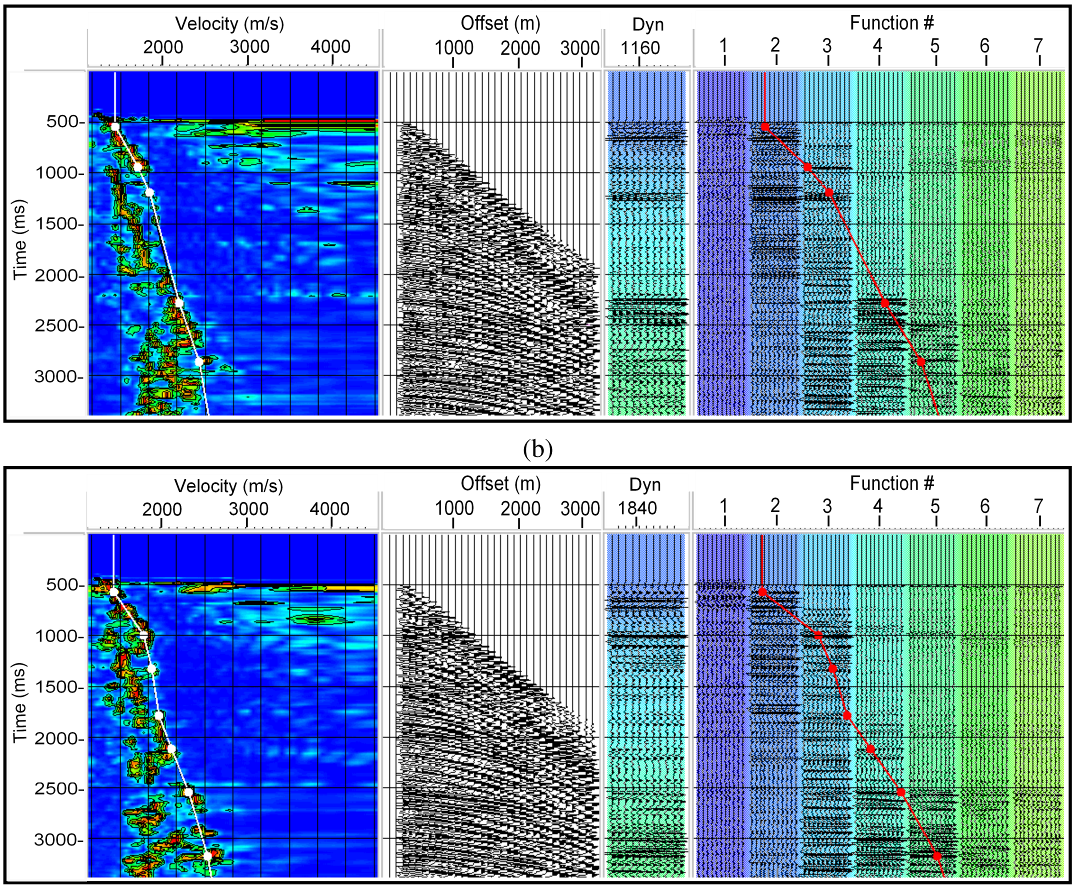

Figure 4: Conventional velocity analysis for (a) CMP 1163 and (b) CMP 1843.

Conventional velocity analysis

For comparison, we performed a conventional processing of the Viking-Graben data to obtain a post-stack time and depth-migrated images and the corresponding velocity models. These serve as a benchmark to evaluate the quality of the corresponding results from RDM processing. As a reference image of the Viking Graben, we used the time-migrated image of Gislain and McMechan (2003).

We carried out a velocity analysis at every 50 midpoints using conventional CMP semblance velocity analysis with velocity spectra ranging from 1500 m/s to 3000 m/s. Figure 4 shows the semblance velocity analysis for CMP 1163 and CMP 1843. The stacking velocity model was created by interpolation. After a first stack, we performed a second velocity analysis to improve the NMO correction. Figure 5 shows the RMS velocity model and NMO-stacked section resulting from conventional processing.

RESULTS OF RDM PROCESSING

To test our RDM processing sequence for these real data, we applied it in two different ways. As a first test, we started from the conventional stacked section of Figure 5. In the second test, we used the nearest-offset section as the starting point.

RDM processing of a conventional NMO-stacked section

After constructing the NMO-stacked section by means of conventional processing, we applied the RDM processing sequence to this zero-offset section. The first step consists of the estimation of the local slopes (see Figure 6a) needed for the PWD filter to reduce the reflection energy. Figure 6b shows the windowed

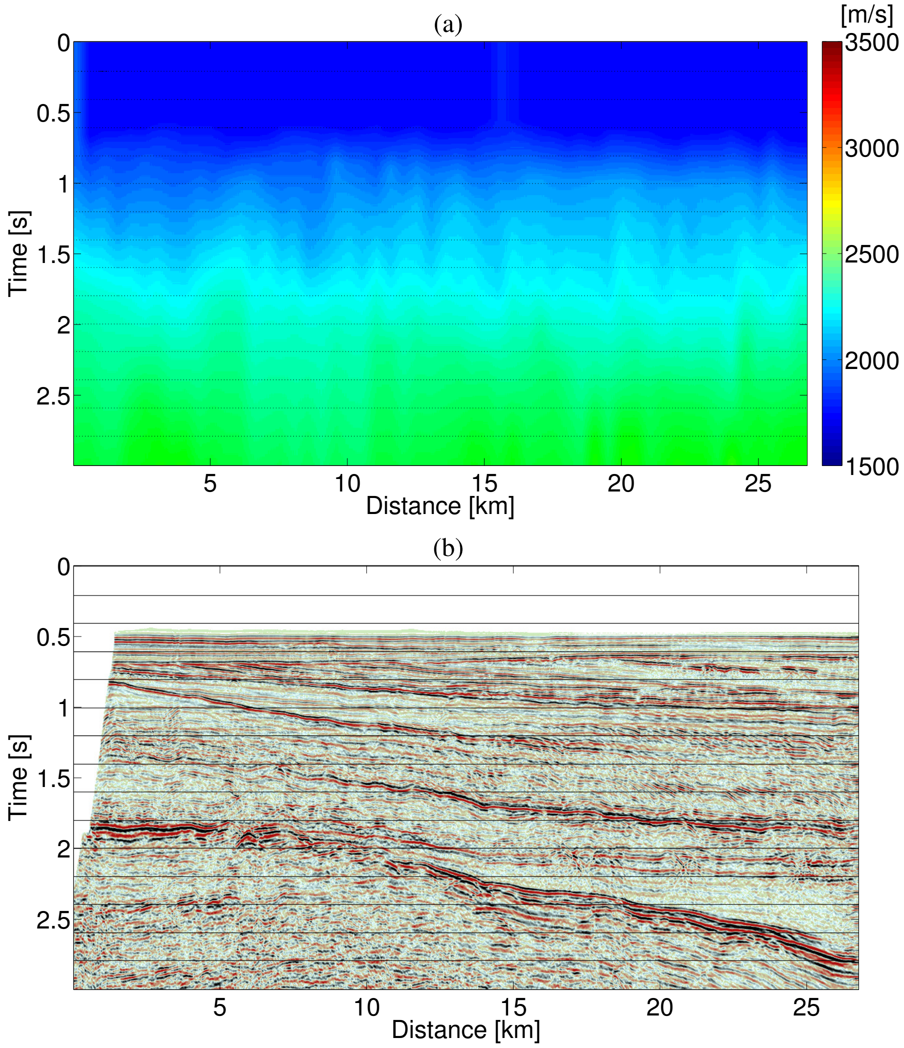

Figure 5: Conventional processing. (a) RMS velocity model. (b) NMO-stacked section.

seismic section with reduced reflections. Note that though the suppression of reflection events is not perfect, many diffractions become visible (compare to Figure 5b).

As previously mentioned, an RDM velocity analysis uses the information contained in the residual moveout of incorrectly migrated diffractions to update the velocity model. According to the theory of Coimbra et al. (2013), the RDM method requires the diffractions to be located in the migrated depth domain. Therefore, we performed a Kirchhoff depth migration on the diffraction section of Figure 6 using (constant) water velocity ($v_0 = 1500$ m/s). The result is shown in Figure 7a. We can identify a number of undermigrated diffractions in the depth domain. To better visualize the diffractions we windowed the migrated image from 0.8 km to 2 km in depth and from 8 km to 22 km in horizontal distance. This depth section was the input to the RDM method. Figure 7b shows the identified and interpreted migrated diffraction events together with the remigration trajectories connecting their positions to their correct depth locations. The corresponding average velocity for this location is then attributed to the focus point of these remigration trajectories.

Following the procedure of Coimbra et al. (2013), we next applied the RDM velocity analysis to the undermigrated section shown in Figure 7a. For this purpose, we selected a window around each interpretable diffraction event to determine its location and to detect its residual moveout. With this information, we trace the associated remigration trajectories and update the velocity v_0 at their focus point. We then interpolate the resulting updated velocity values at all interpreted diffraction events to find an average depth

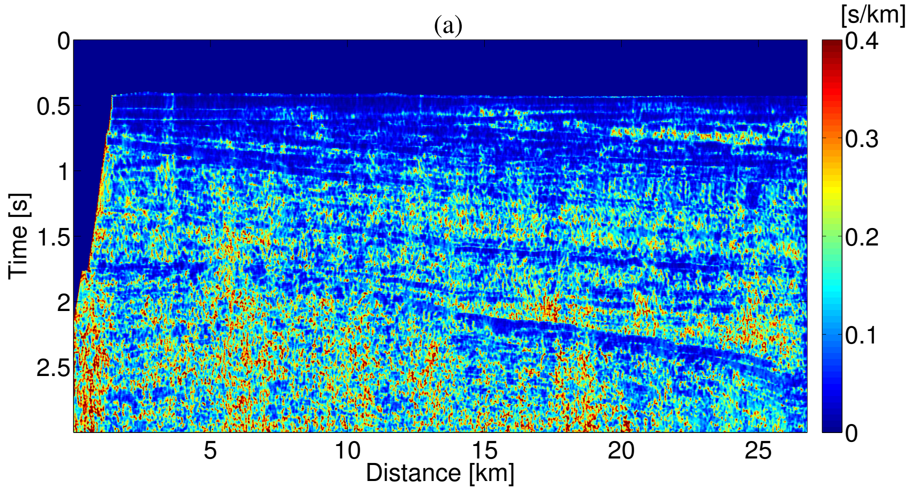

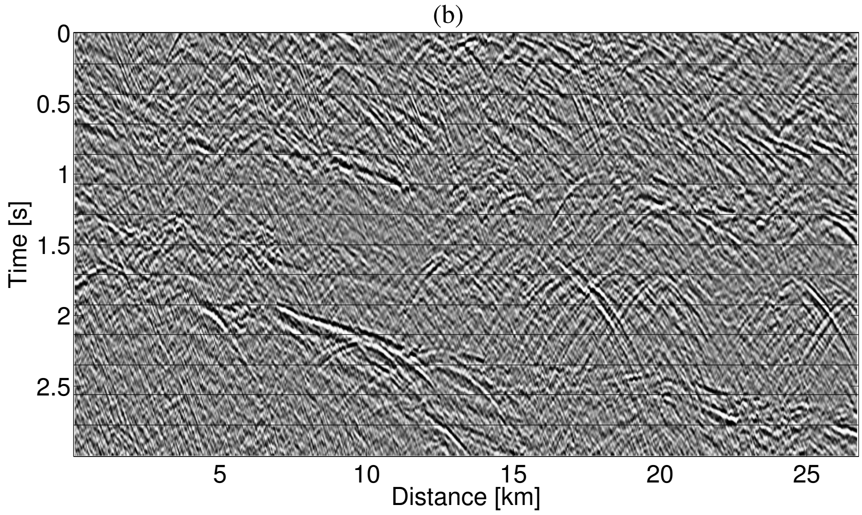

Figure 6: RDM processing starting with a ZO section. (a) Local slopes. (b) Diffraction filtered section.

velocity model, which is then converted to an RMS velocity model (Figure 8a). With this new velocity model, we have carried out a post-stack Kirchhoff time migration, shown in Figure 8b.

The RMS velocity model obtained by this procedure (Figure 8a) is slightly smoother than the one from conventional velocity analysis (Figure 5a), and presents a little higher velocities. The time-migrated image is of acceptable quality, indicating that the velocity model represents the true velocities sufficiently well.

Of course, it is somewhat unsatisfactory to construct another RMS velocity model after a conventional velocity analysis already has been carried out. This section is meant to demonstrate that diffracted energy can be isolated in real data, and that it contains sufficient velocity information for a velocity-model construction. In the next section, we replace the input NMO-stacked section by the nearest-offset section to demonstrate that RDM processing can be applied independently of a previous velocity analysis.

RDM processing starting with the nearest offset

After many tests, we were finally able to set up a processing sequence that allows to apply the residual diffraction moveout migration velocity analysis of Coimbra et al. (2013) to real data. The procedure starts with the nearest avalable common-offset section. Important measures that make the process work include suitable data selection, reliable estimation of the local slope, and the application of the PWD filter to reduce reflected energy in the data. Together with the iterative application of the RDM analysis, these steps were fundamental to achieving good results. As mentioned earlier, we refer to the whole processing sequence,

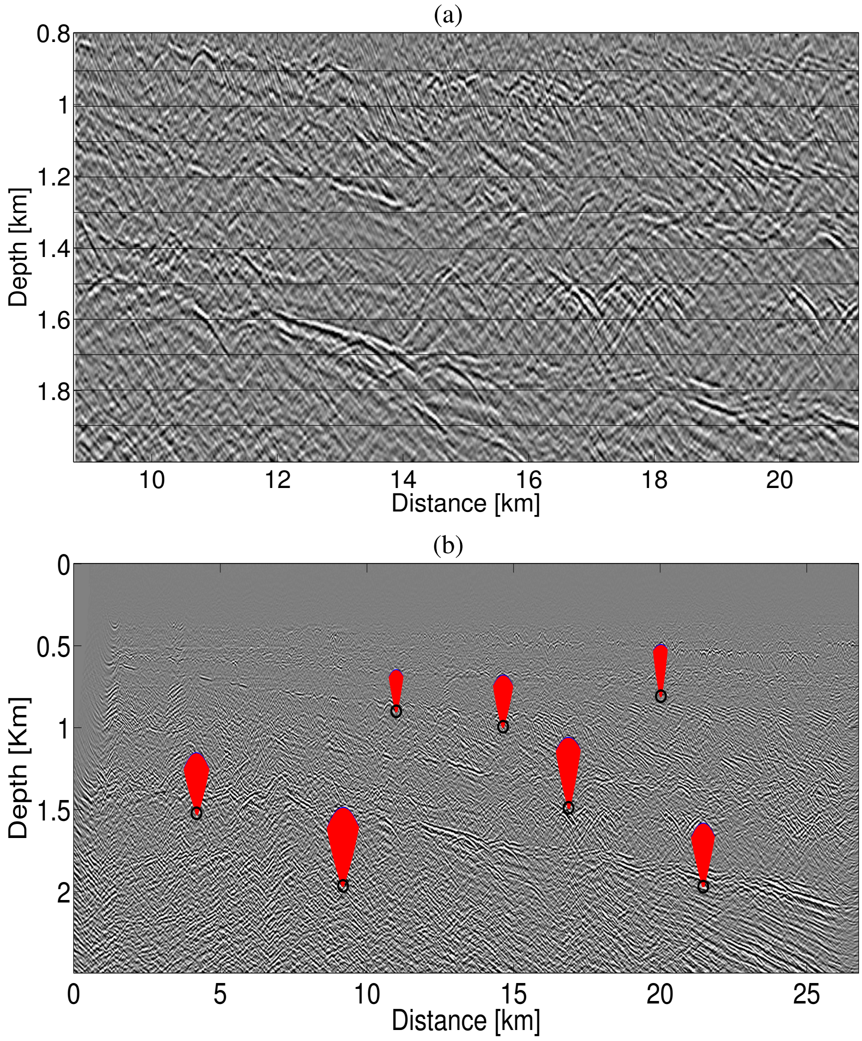

Figure 7: RDM processing of a ZO section. (a) Depth migration with velocity v_0=1500 m/s (produces undermigrated diffractions) after applying the PWD filter. (b) Interpreted diffraction events and their remigration trajectories (red lines forming apparent cones).

composed of local-slope estimation, PWD filter, and iterative moveout analysis, as RDM processing. In our application, we were able to construct velocity models in both the time and depth domains. The necessary steps of post-stack time migration, post-stack depth migration, and pre-processing were carried out with conventional tools.

Our RDM processing sequence starts with an application of the local-slope estimation to the nearest-offset section available in the data. These slopes are then used to apply the PWD filter to reduce reflection energy in the data section and make the diffraction events more easily identifiable. This, in turn, allows for the first iteration of the RDM velocity analysis as described in (Coimbra et al., 2013), starting with a constant-velocity migration. The updated RMS velocity model allows to carry out an NMO stack to produce a first estimate of the zero-offset section. The following iterations start with the velocity model and stacked section of the preceeding iteration.

First iteration The theory of Coimbra et al. (2013) requires a zero-offset (ZO) section as input to the RDM velocity analysis. However, at the start of seismic processing, such a section is not available. Therefore, we started at the nearest-offset section. The use of a finite-offset section instead of a zero-offset one

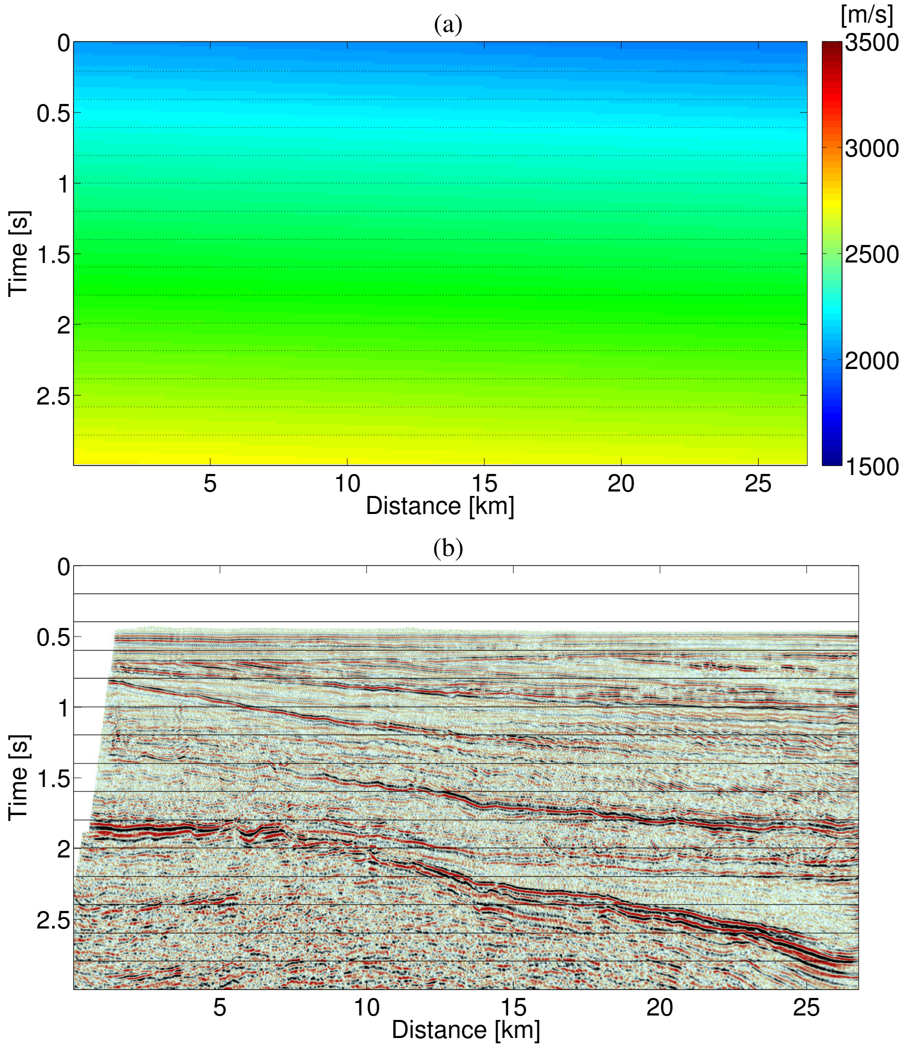

Figure 8: RDM processing of a ZO section. (a) RMS velocity model. (b) Time migrated image.

will lead to an error in the resulting velocity model. As we will see below, this error is sufficiently small to be accepted in the first iteration. It is then reduced by the following iterations that act on NMO-stacked sections.

In the Viking Graben dataset the smallest offset is 262 m (see Figure 9a). Because of the amplitude difference between reflections and diffractions, the latter are hardly visible in this section.

As in the case of the stacked section above, the application of a PWD filter with the extracted local-slope values (see Figure 9b) achieved sufficient suppression of the reflection energy, so that diffraction events become visible and interpretable (see Figure 9c). Note that the slope section itself can be helpful for the identification of diffraction events, because their slope values tend to be higher than those of reflections (see again Figure 9b).

In the same way as in the case of the NMO-stacked section, we applied Kirchhoff depth migration with water velocity ($v_0 = 1500$ m/s) to the diffraction section of Figure 9c. The result is shown in Figure 10a. To better visualize the diffractions, we windowed the migrated image from 0.8 km to 2 km in depth and from 8 km to 22 km in horizontal distance. Though the reflector images are still predominant in this figure, it is still possible to identify and interpret a number of undermigrated diffractions. Figure 10b shows the complete migrated diffraction section with remigration trajectories (red lines) used to update the first velocity v_0. The resulting updated RMS velocity model is depicted in Figure 11a.

We recognize the velocities to be in a similar range as the ones from the conventional velocity analysis

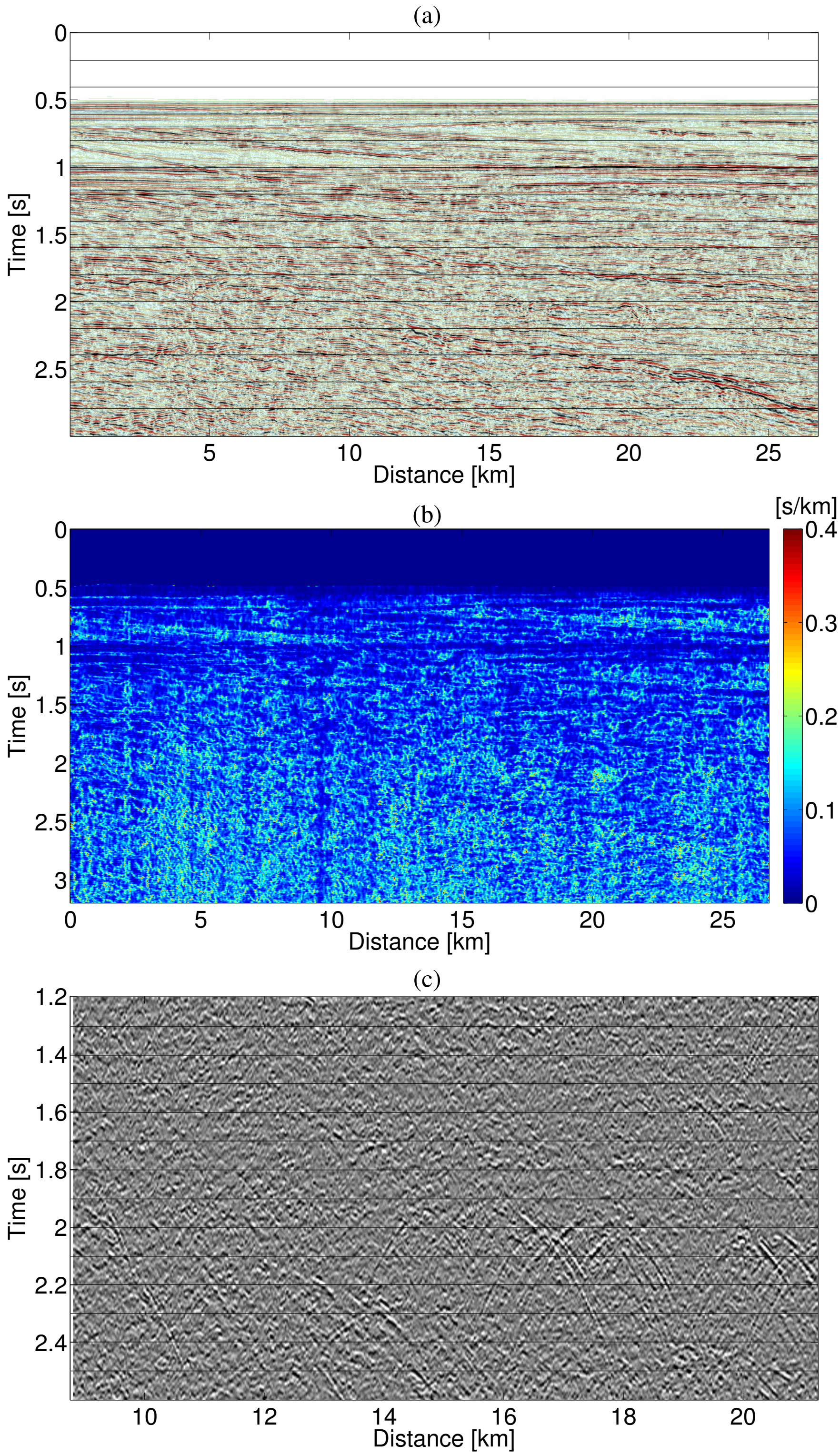

Figure 9: First iteration of RDM processing. (a) Input: Nearest-offset section. (b) Local slopes of the nearest-offset section. (c) Nearest-offset section after suppression of reflections (cental part, between 8 km and 22 km horizontally and between 1.2 s and 2.6 s in time).

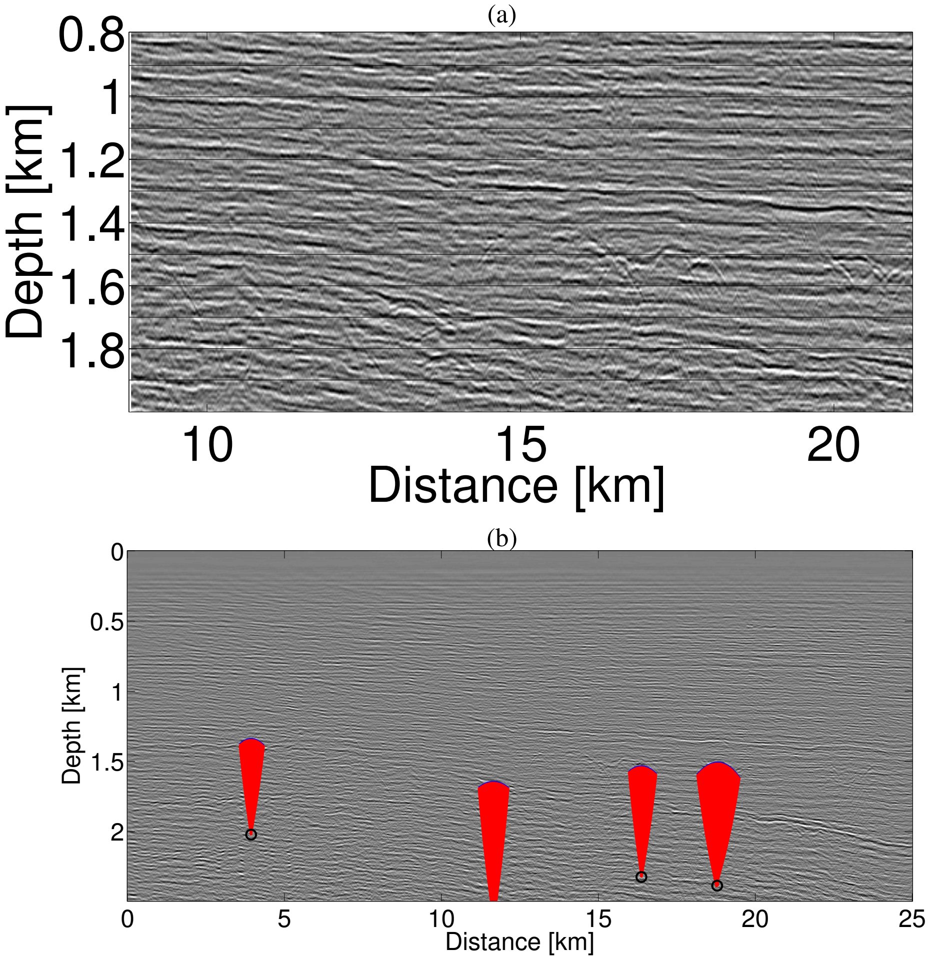

Figure 10: First iteration of RDM processing. (a) Depth migrated nearest-offset section after application of a PWD filter. Migration velocity was water velocity $v_0 = 1500$ m/s. (b) Identified and interpreted undermigrated diffractions with remigration trajectories (red lines).

(Figure 5a). However, the velocity field is smoother in the horizontal direction. Using this updated RMS velocity model, we applied an NMO correction to the complete Viking-Graben dataset and stacked the so-corrected data. The resulting NMO-stacked section (Figure 11b) is the input to the second iteration of RDM processing.

As we can see at the left-hand side of Figure 11b, the reflectors are not well positioned, indicating poor model quality in this region. The reason is that we were not able to identify any diffractions in this part of the data in the first iteration of RDM processing. It is important to notice that this is not an important issue at this stage, because it can be remedied in future iterations. Our particular interest for the next iteration is to identify additional diffractions in these parts of image.

Second iteration The next step is the slope extraction in this approximate stacked zero-offset section of Figure 11b. The resulting slope section is depicted in Figure 12a. From a comparison to Figure 9b, we immediately observe that the slopes of the reflection events are better estimated, because now the structure of the data is much better visible in the slope section. As a consequence, the reflected energy is better removed by the PWD filter (see Figure 12b), so that more diffraction events can be identified.

For the depth migration of the diffraction section of Figure 12b, we need an interval velocity model. Since our velocity values are local average velocities obtained from a remigration-based techniques, we use the method proposed by Schleicher et al. (2004) to convert these velocities to interval velocities. Figure 13a

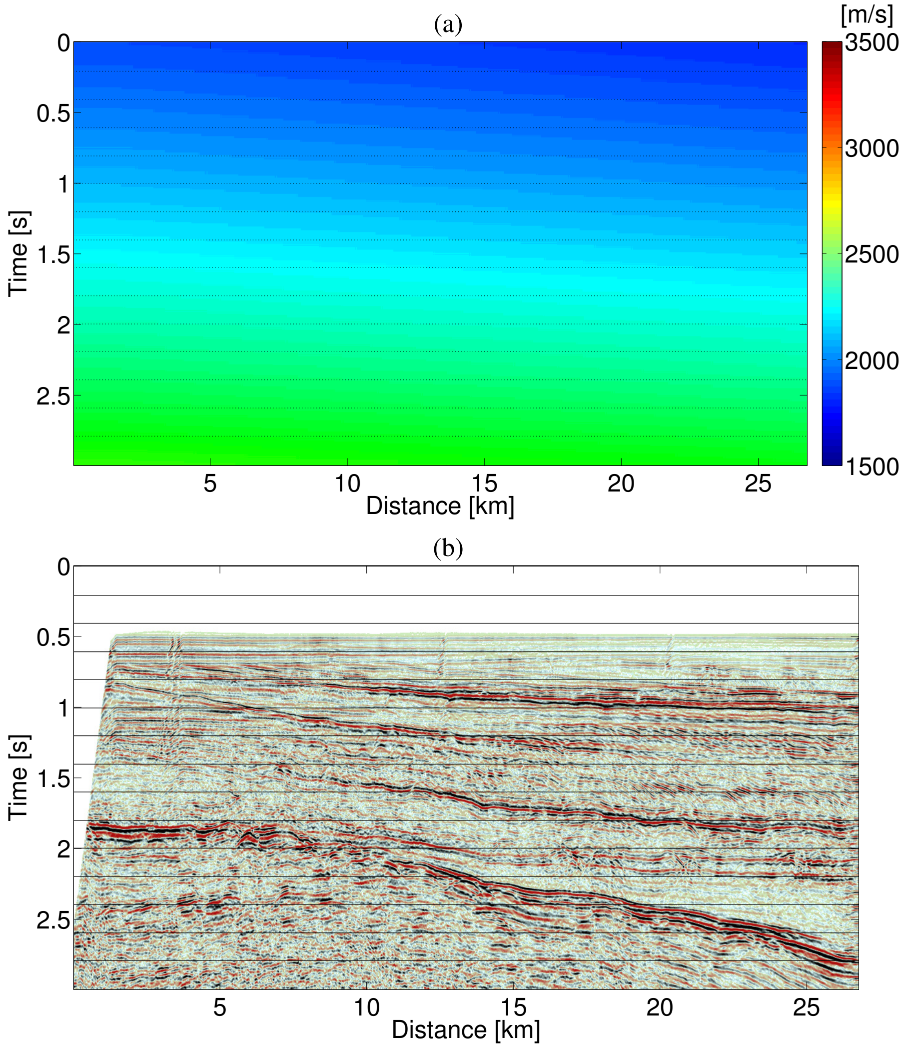

Figure 11: First iteration of RDM processing. (a) RMS velocity model. (b) NMO- stacked section. This is the output from the first iteration and becomes the input to the second iteration.

shows the central part (8 km to 22 km horizontally, 0.8 s to 2.0 s vertically) of the Kirchhoff-migrated depth section with the so-obtained interval velocity model. Several uncollapsed diffraction events are identifiable. Figure 13b shows the total migrated section with identified diffractions and their corresponding remigration trajectories. The focusing velocities of these trajectories define again the velocity updates at the focus points.

Finally, with the velocity model found in the second RDM iteration (see Figure 14a), we constructed a new NMO-stacked section (Figure 14b). This stacked section has visibly improved over the one from the previous iteration (Figure 11b). The reflectors at the top of the section show better continuity and the deeper ones are better focused. In other words, the initial error, caused by using the nearest-offset section, was overcome by the second iteration.

After establishing the velocity models in the time and depth domains using conventional velocity analysis and the RDM processing, we performed post-stack time and depth Kirchhoff migrations. In both cases, we used a maximum frequency of 50.0 Hz, and also kept all other parameters identical. For better visualization, we show the central windows of the resulting images

Figure 15 shows the post-stack time-migrated sections with the conventional velocity model (15a) and the RDM model (15b). As can be noted, inspite of the differences in the velocity models, the results are quite similar. The conventional image in Figure 15a presents more focused reflectors, but their local lateral

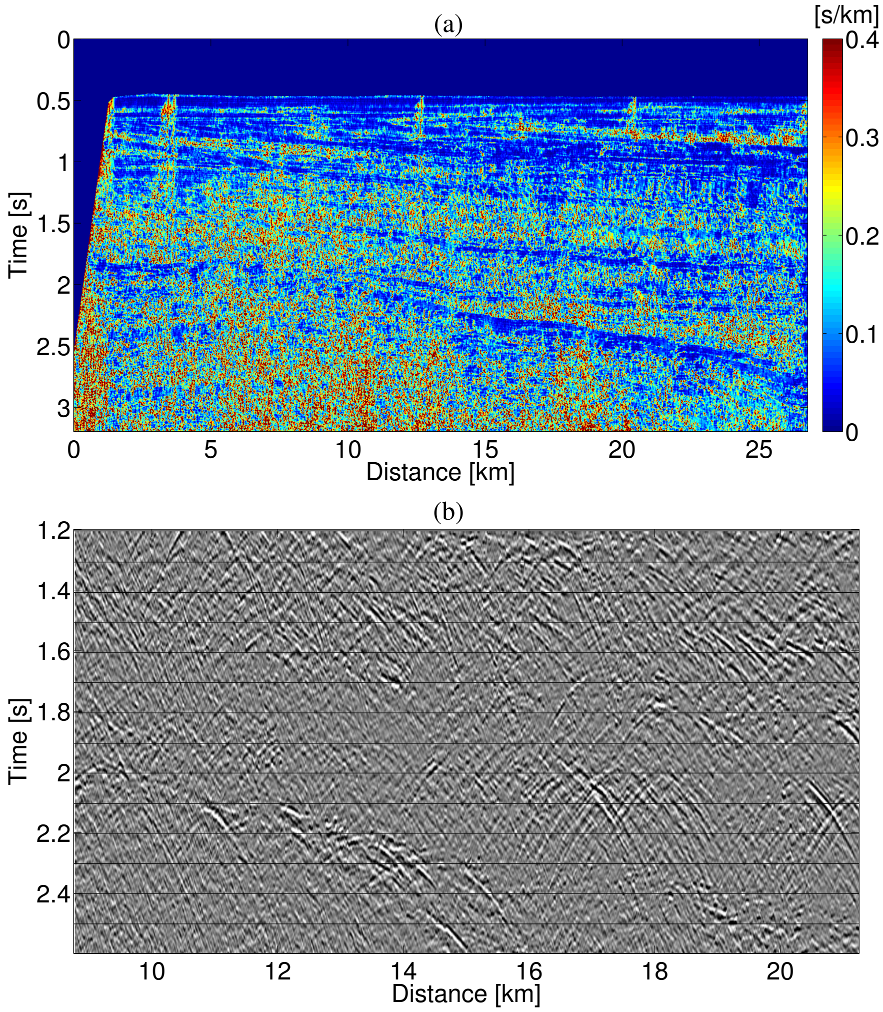

Figure 12: Second iteration of RDM processing. (a) Local slopes of the NMO-stacked section. (b) PWD filtered NMO-stacked section (central part).

variation are a little stronger, and the reflector elements below 2.2 s in the left part of the image are not visible at all. In contrast, the reflectors in the time migration with the RDM velocity (Figure 15b) are a little weaker but smoother, and the reflector elements in the bottom left corner start to become interpretable.

Figure 16 shows the interval velocity models from conventional and RDM processing. We converted the average velocity from the RDM method to interval velocity using vertical slowness averages (Schleicher et al., 2004), and the RMS velocities from conventional processing using Dix conversion (by PROMAX). In both cases, we did not consider any lateral variations. Note that the interval velocity from RDM processing presented a better correlation with layers in the seismic section than the conventional velocity. An important difference between the models is the determined velocity at depths greater than 2 km. The RDM velocity increases faster than the conventional velocity. This behavior has a measurable effect on the position of the reflectors in depth migration. The conventional model can be postprocessed to improve the correlation with the seismic layers, but that will require more processing time compared with the RDM processing.

With the velocity models in the depth domain from the RDM and conventional processing, we performed Kirchhoff depth migrations (Figure 17). The resulting images show little differences in the structures, except for the depth positioning of the reflectors. Though in the conventional image (Figure 17a), the reflectors again are slightly better focused, the RDM image (Figure 17b) shows an improved location of faults. This indicates that the velocity model found in the second iteration of the RDM processing is of acceptable quality.

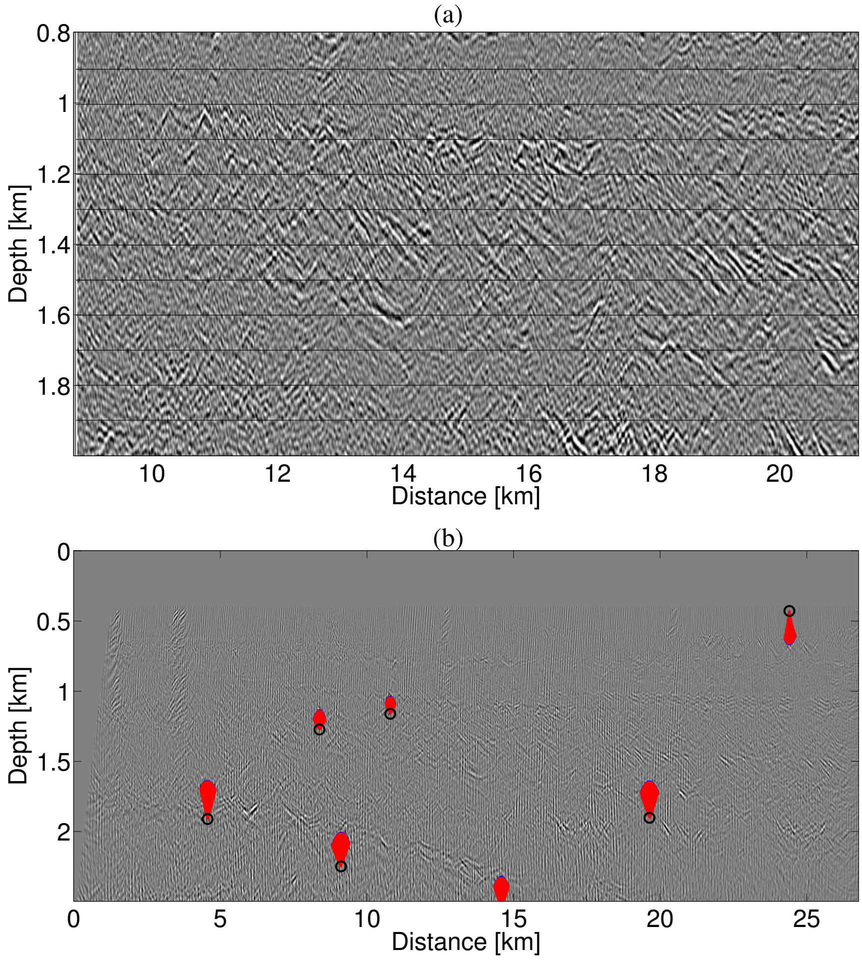

Figure 13: Second iteration of RDM processing. (a) Depth migration of the filtered diffraction section, obtained using with the velocity model from the first iteration. (b) Undermigrated diffraction curves with remigration trajectories (red lines).

Like the conventionally obtained model from time-domain velocity analysis, also the RDM model should be considered a starting model for more sophisticated migration-velocity-analysis techniques. If required, its quality can be improved by better adjustment of some of the parameters. For example, the restriction of purely vertical velocity variations should probably be dropped. Possibly, better techniques for local-slope estimation, diffraction filtering or velocity interpolation may also help to improve the result. However, it is to be kept in mind that the model building using RDM processing was considerably faster than conventional velocity analysis, due to the restrictions used and the small number of diffractions (eleven) required to reach a suitable velocity model. However, for a more complex dataset or 3D data, manual diffraction picking will become more expensive. Automatic picking procedures must be considered to make RDM processing feasible in such situations.

CONCLUSION

In this paper we have constructed a new processing flow for velocity analysis based on the residual-moveout analysis of incorrectly migrated diffraction events of Coimbra et al. (2013). A key element of our processing sequence is the attenuation of reflected energy by means of plane-wave-destruction (PWD) filters.

The identification of diffractions in a real dataset is a difficult task in the seismic processing, because of the weak energy of diffractions compared with reflections and sometimes even the noise. In our implemen-

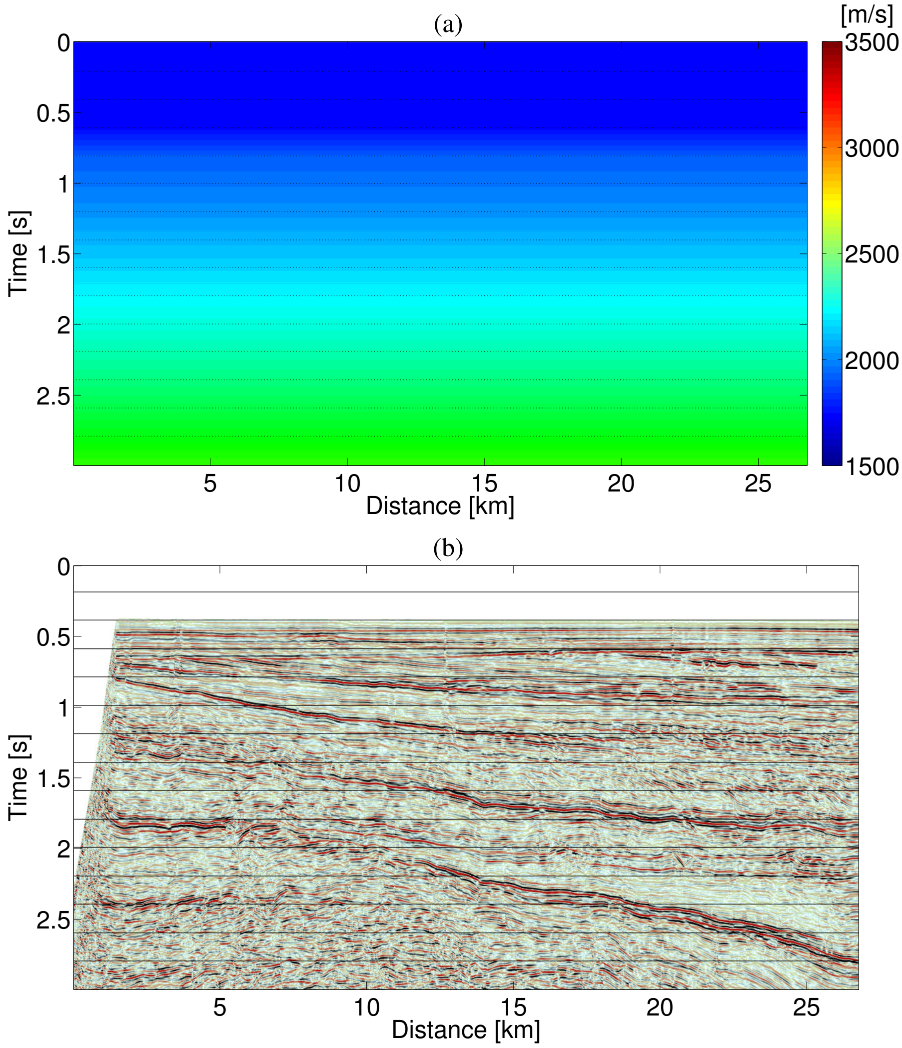

Figure 14: Second iteration of RDM processing. (a) RMS velocity model. (b) NMO- stacked section.

tation of a modified PWD filter, we have used the improved local-slope extraction technique of Schleicher et al. (2009) to separate diffractions from reflections. Even though the suppression of reflection events by the PWD filter is not perfect, it helps to make more diffractions visible and interpretable.

To test the new residual-diffraction-moveout (RDM) processing sequence, we have applied it to a real seismic data set from the Viking Graben in the North Sea, provided by Exxon Mobil. In the first application, we started at an NMO-stacked section obtained after conventional velocity analysis. In a more realistic test, we started at the nearest-offset section available from the data. In both tests, we were able to construct acceptable velocity models for time and depth migration. Although Coimbra et al. (2013) had developed the RDM velocity-analysis technique for zero-offset migration, the error from starting at the nearest-offset section was sufficiently small not to affect subsequent iterations. For the Viking Graben seismic data, only two iterations were sufficient to arrive at an acceptable velocity model.

To analyse the quality of the obtained velocity models in time and depth, we compared the resulting seismic migrated images to those obtained by conventional seismic processing. As our results showed, the velocity models in the time and depth domains obtained from the RDM processing produced migrated images of similar quality as the ones from the conventional method in considerably less turnaround time. For the Viking Graben dataset, we arrived at a satisfactory migration-velocity model in an overall processing time of a single work day, while the conventional semblance analysis took four days to complete.

It is important to emphasize that we do not aim at suggesting that our methodology is better or worse

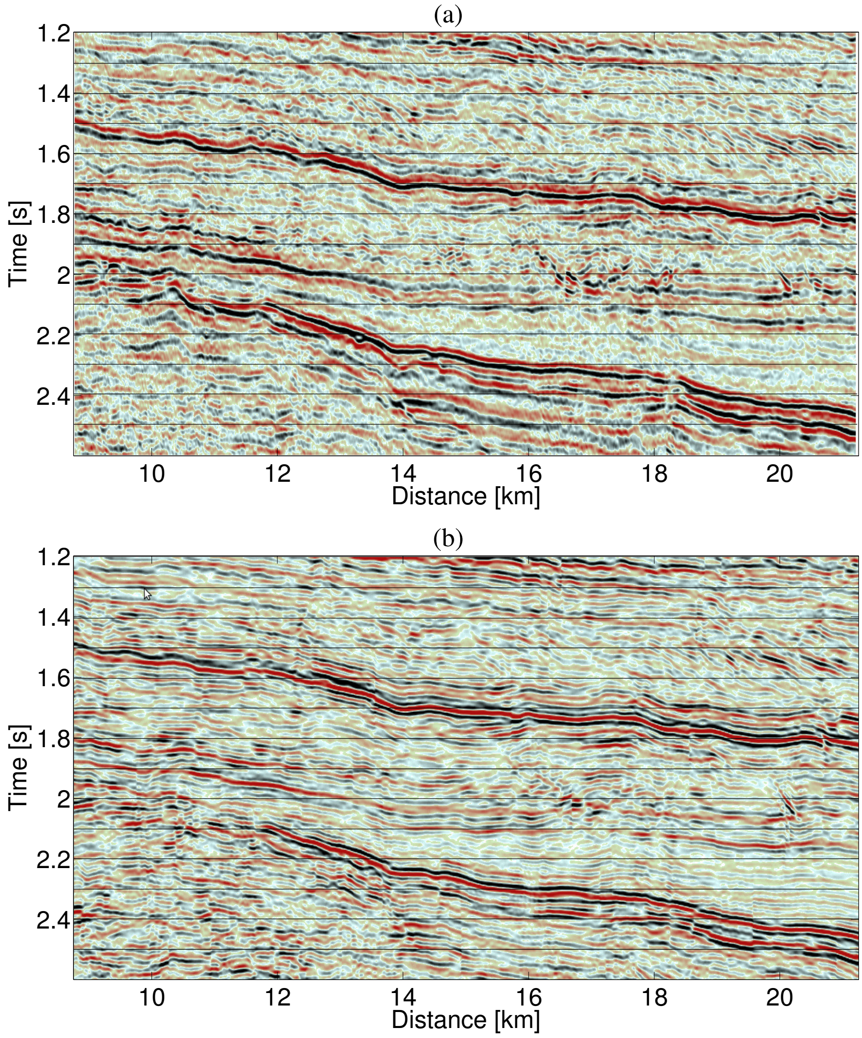

Figure 15: Time migrated sections with the model from (a) conventional processing and (b) RDM processing. The original seismic sections were windowed horizontally (from 0.8 km to 22 km) and in time (from 1.2 s to 2.6 s) for better visualization.

than conventional methodologies. We are simply trying to point out that there are promising alternatives to conventional processing. Considering diffractions might help to extract additional information from the data which is not made use of in conventional processing. With our workflow, it was possible in the case of a real Viking Graben dataset to construct an acceptable velocity model purely from diffraction information. In more complicated situations, a combination of diffraction and reflection information might still be superior to using reflections alone.

While it is hard to quantify the seismic processing time, especially when the time depends on human interaction, our workflow has demonstrated that the information contained in diffraction events can be made accessible in a fraction of the time needed for conventional processing. Note that also in this aspect, the diffraction filtering was essential because a part of the processing time in our procedure is spent on the identification and interpretation of diffractions.

ACKNOWLEDGMENTS

The authors thank the Exxon Mobil for providing the Viking Graben dataset and SMAART-JV for the Sigsbee2B data and model. This work was kindly supported by the Brazilian agencies CAPES, FINEP, and

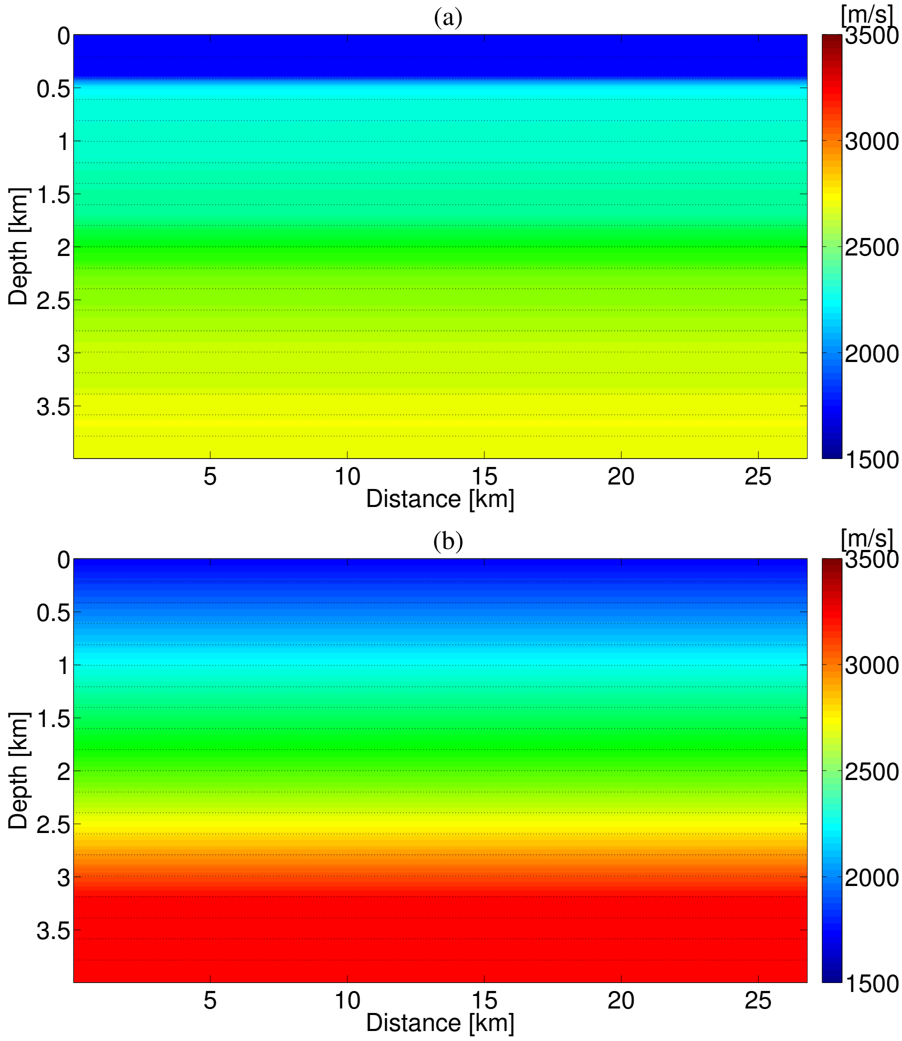

Figure 16: Final depth velocity model from (a) conventional velocity analysis and (b) RDM processing.

CNPq, as well as Petrobras and the sponsors of the Wave Inversion Technology (WIT) Consortium.

REFERENCES

Alonaizi, F., Pevzner, R., Bóna, A., Alshamry, M., Caspari, E., and Gurevich, B. (2014). Application of diffracted wave analysis to time-lapse seismic data for CO2 leakage detection. *Geoph. Prosp.*, 62(2):197–209.

Alonaizi, F., Pevzner, R., Bóna, A., Shulakova, V., and Gurevich, B. (2013). 3D diffraction imaging of linear features and its application to seismic monitoring. *Geoph. Prosp.*, 61(6):1206–1217.

Claerbout, J. F. (1992). *Earth soundings analysis – processing versus inversion*. Blackwell Scient. Publ.

Coimbra, T. A., de Figueiredo, J. J. S., Schleicher, J., Novais, A., and Costa, J. C. (2013). Migration velocity analysis using residual diffraction moveout in the poststack depth domain. *Geophysics*, 78(3):S125–S135.

Fomel, S. (2009). Applications of plane-wave destruction filters. *Geophysics*, 67:1946–1960.

Gislain, B. M. and McMechan, G. A. (2003). Processing, inversion, and interpretation of a 2D seismic data set from the North Viking Graben, North Sea. *Geophysics*, 68(3):837–848.

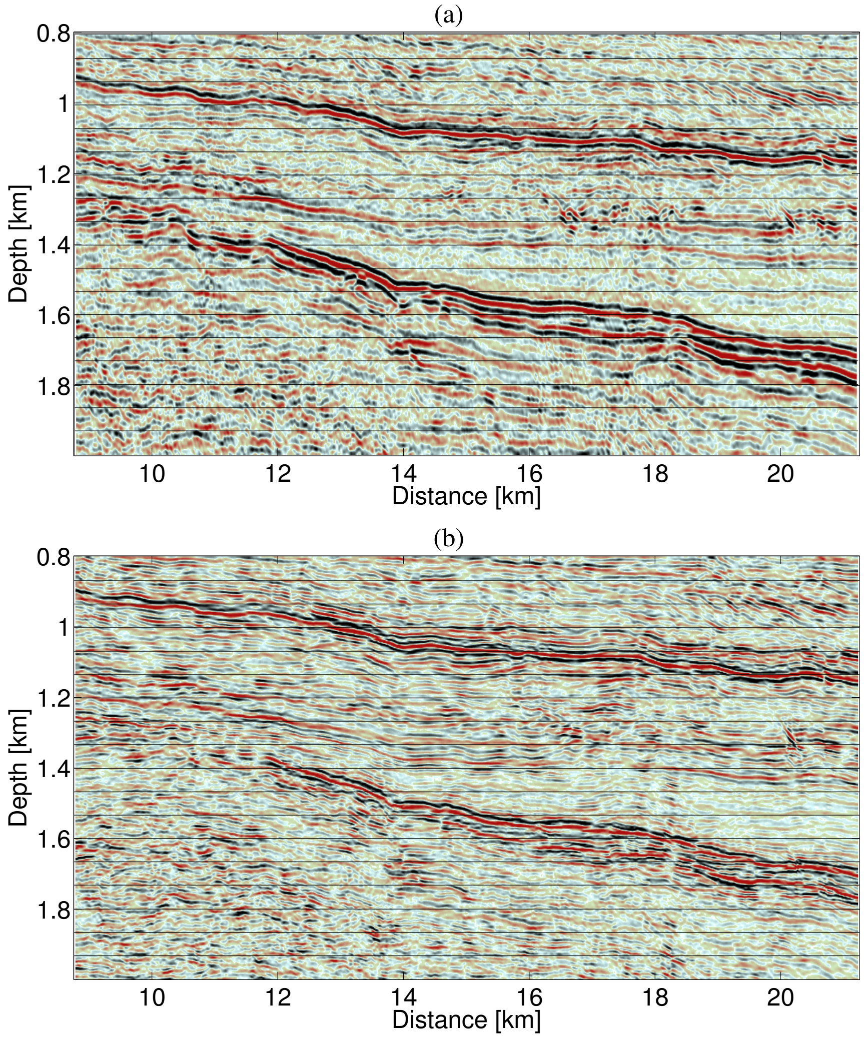

Figure 17: Depth-migrated sections with interval models from (a) conventional processing and (b) RDM processing. The images were windowed horizontally (0.8 km to 22 km) and in depth (1.2 km to 3.0 km).

Hale, D. (2007). Local dip filtering with directional Laplacians. *CWP Report*, 567.

Hubral, P., Tygel, M., and Schleicher, J. (1996). Seismic image waves. *Geoph. J. Int.*, 125:431–442.

Khaidukov, V., Landa, E., and Moser, T. J. (2004). Diffraction imaging by focusing-defocusing: An outlook on seismic superresolution. *Geophysics*, 69(6):1478–1490.

Landa, E. and Reshef, M. (2009). Separation, imaging, and velocity analysis of seismic diffractions using migrated dip-angle gathers. In *79th Ann. Internat. Meeting, SEG, Expanded Abstracts*, pages 2176–2180.

Novais, A., Costa, J., and Schleicher, J. (2008). GPR velocity determination by image-wave remigration. *Journal of Applied Geophysics*, 65:65–72.

Sava, P., Biondi, B., and Etgen, J. (2005). Wave-equation migration velocity analysis by focusing diffractions and reflections. *Geophysics*, 70(3):U19–U27.

Schleicher, J., Costa, J. C., Santos, L. T., Novais, A., and Tygel, M. (2009). On the estimation of local slopes. *Geophysics*, 74:25–33.

Schleicher, J., Novias, A., and Munerato, F. (2004). Migration velocity analysis by depth image-wave remigration: First results. *Geoph. Prosp.*, 52:559–573.

Tsingas, C., Marhfoul, B. E., Satti, S., and Dajani, A. (2011). Diffraction imaging as an interpretation tool. *First Break*, 29:57–61.

Zhang, R. (2004). Imaging the earth using seismic diffractions. CDSST annual report.